PAPER • OPEN ACCESS

Magnetization dynamics of magnetic domain wall imprinted magnetic films

To cite this article: Christine Hamann *et al* 2014 *New J. Phys.* **16** 023010

View the article online for updates and enhancements.

Magnetization dynamics of magnetic domain wall imprinted magnetic films

Christine Hamann[1]**, Roland Mattheis**[2]**, Ingolf Mönch**[3]**, Jürgen Fassbender**[4]**, Ludwig Schultz**[1] **and Jeffrey McCord**[1,4,5,6]

[1] Institute for Metallic Materials, IFW Dresden, PO Box 270116, D-01171 Dresden, Germany
[2] Institute of Photonic Technology Jena, PO Box 100239, D-07702 Jena, Germany
[3] Institute for Integrative Nanosciences, IFW Dresden, PO Box 270116, D-01171 Dresden, Germany
[4] Institute of Ion Beam Physics and Materials Research, Helmholtz-Zentrum Dresden-Rossendorf, PO Box 510119, D-01314 Dresden, Germany
[5] Institute for Materials Science, Kiel University, Kaiserstraße 2, D-24143 Kiel, Germany
E-mail: jmc@tf.uni-kiel.de

Abstract

The influence of micromagnetic objects on the dynamic magnetic excitation in magnetic thin films is studied by imprinting periodic domain wall patterns through selective ion irradiation in exchange biased $Ni_{81}Fe_{19}$/IrMn structures. For high domain wall densities an increased precessional frequency is achieved. The zero field resonance of the domain wall state hereby depends directly on the stripe period, showing a pronounced increase with decrease of domain wall spacing. With the abrupt annihilation of magnetic domain walls with an applied bias field a jump-like decrease in precessional frequency takes place. The experimental data and micromagnetic simulations prove that the characteristic collective dynamic mode for the domain wall configurations is attributed to strongly coupled tilted magnetization structure. This is evidenced by an overlapping Néel wall structure for the narrowly spaced imprinted antiparallel unidirectional anisotropy state. The controlled introduction of high density frozen-in micromagnetic objects is a novel way to control the dynamic magnetic properties of continuous magnetic thin films.

[6] Author to whom any correspondence should be addressed.

1. Introduction

The dynamic magnetic behavior of magnetic films has gained increased attention due to the raised data rate in magnetic recording [1], the use of magnetic films for high frequency inductors [2, 3] and their application as microwave filters [4, 5]. Moreover, the excitation and modification of spin waves has led to considerable interest in the field of magnonic crystals [6–9]. In general, the high frequency behavior of magnetic film stacks is determined by the material's magnetic properties. On the other hand secondary effects such as structural patterning, through magnetic shape anisotropy, and exchange bias coupling in magnetic multilayers [10–12] have considerable effects on the dynamic magnetic functionality or spin wave propagation in the films. Switchable dynamic properties are achieved with nano-patterned stripes with varying magnetic ground states [13, 14]. Yet, dynamic magnetization modes are not only inherent to the physical structure of magnetic films, but are also strongly influenced by e.g. magnetic ripple or blocked magnetic domain states [15, 16]. Moreover, the existence itself of domain walls (DWs) proved to have influence on the dynamic properties and the dynamic permeability spectra [17, 18] of magnetic films. Néel-type DWs in thin films consist of a narrow width core with a width below the thickness of the magnetic film and a wide tail region, the width of which is determined by the ratio of magnetic charges and uniaxial anisotropy energy density [19]. In the Néel tails the magnetization component perpendicular to the DW decays logarithmically over a wide distance, thus leading to a strong magnetic interaction of narrowly spaced Néel walls. In order to study the influence of the magnetic DWs on the dynamic magnetization behavior of magnetic thin films, DWs need to be positioned in a controlled way within the magnetic thin film structure. Yet, the reproducible nucleation and positioning of magnetic DWs in a high density arrangement are difficult to achieve in regular magnetic films.

Here, we present results on extended exchange biased [20, 21] $Ni_{81}Fe_{19}/IrMn$ films with periodically alternating directions of exchange bias. The magnetically hybrid structures with antiparallel unidirectional anisotropy directions are unique as, e.g. a domain pattern of antiparallel stripe magnetization and DWs can be imprinted directly into the magnetic material [22, 23]. Thus, in dependence of the applied magnetic field amplitude along the easy magnetization direction, the system allows for a defined adjustment of the magnetic configuration with a saturated ferromagnetic magnetization alignment (S) as well as DW configuration state with a high and predefined DW density (figure 1).

2. Experiment and results

The DW array structures were prepared from a continuous dc-sputtered polycrystalline Ta (4 nm)/$Ni_{81}Fe_{19}$ (20 nm)/$Ir_{23}Mn_{77}$ (7 nm)/Ru (3 nm) [11] film under ultra high vacuum conditions on a thermally oxidized Si-wafer substrate. The initial exchange bias direction $H_{eb,dep}$ was set by depositing the films in an external saturation field of $H_{dep} = 3.6\,kA\,m^{-1}$. Magnetization loops were measured by inductive magnetometry at 10 Hz and locally by high resolution magneto-optical magnetometry. The exchange bias field of the according extended reference films amounts to $H_{eb,dep} = 3.7\,kA\,m^{-1}$ (figure 2(a)). In order to obtain a two-dimensional lateral modulation of the unidirectional exchange anisotropy the layer stacks were locally protected by a photoresist mask and subsequently implanted by He^+ ions at 10 keV and an ion fluence of $1.2 \times 10^{15}\,He\,cm^{-2}$ in presence of a magnetic field of $H_{irr} = 8.0\,kA\,m^{-1}$ along the stripe axis, but oriented opposite to the deposition field direction [24, 25]. This ion energy
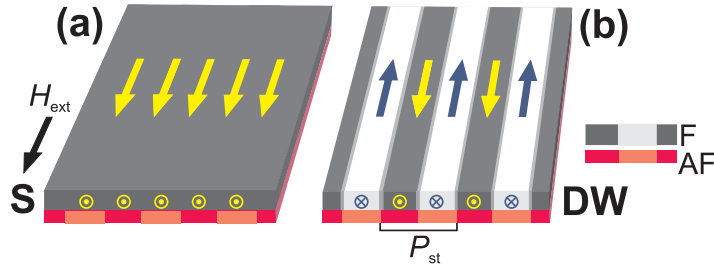
Figure 1. Principle sample structure and magnetization state in the (a) saturated S state and (b) zero applied magnetic field antiparallel DW state. The assumed directions of magnetization and the positions of the Néel walls are sketched.
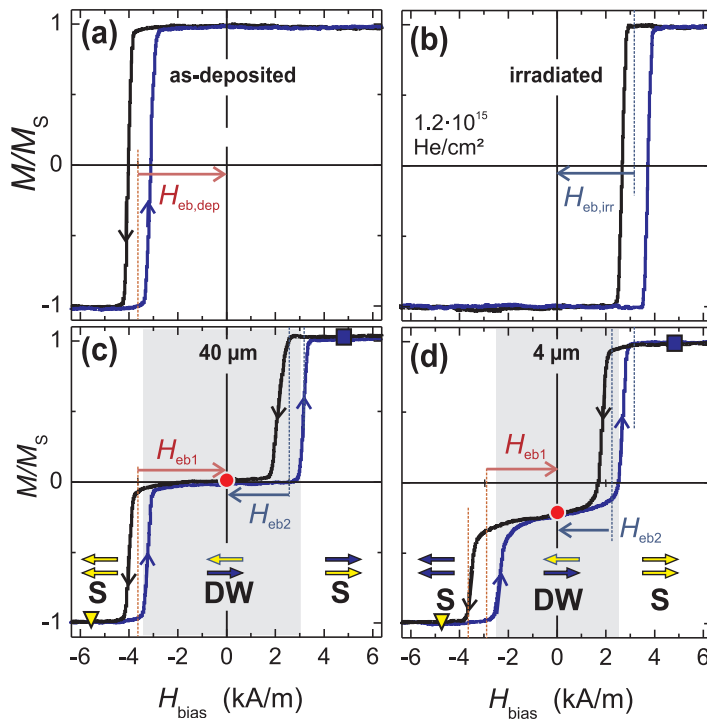
Figure 2. Inductive hysteresis loops for the (a) as-deposited and (b) irradiated full films, and for two characteristic exchange bias modulated film structures with (c) $P_{st} = 40\,\mu m$ and (d) $4\,\mu m$. The S labeled field regions mark states of saturated state magnetization. For external bias fields $-H_{eb1} < H_{bias} < -H_{eb2}$ the structures exhibit nominally antiparallel stripe magnetization or DW state.

allows for the complete penetration of the magnetic layer [26] and reorientation of the induced exchange bias field direction [23, 27] of the irradiated stripes (full film: $H_{eb,irr} = 3.2\,kA\,m^{-1}$, figure 2(b)). The extended stripe arrays are $10 \times 10\,mm^2$ in dimension, while the stripe period P_{st} is varied from 40 down to $2\,\mu m$, the latter resulting in 10^4 well aligned DWs within the sample.

Applying the magnetic field along the easy directions of magnetization, the mixed property structures exhibit a two-step magnetic hysteresis loop with an intermediate magnetization plateau at low external bias fields H_{bias} limited by $H_{eb,dep}$ and $H_{eb,irr}$ (figures 2(c) and (d))
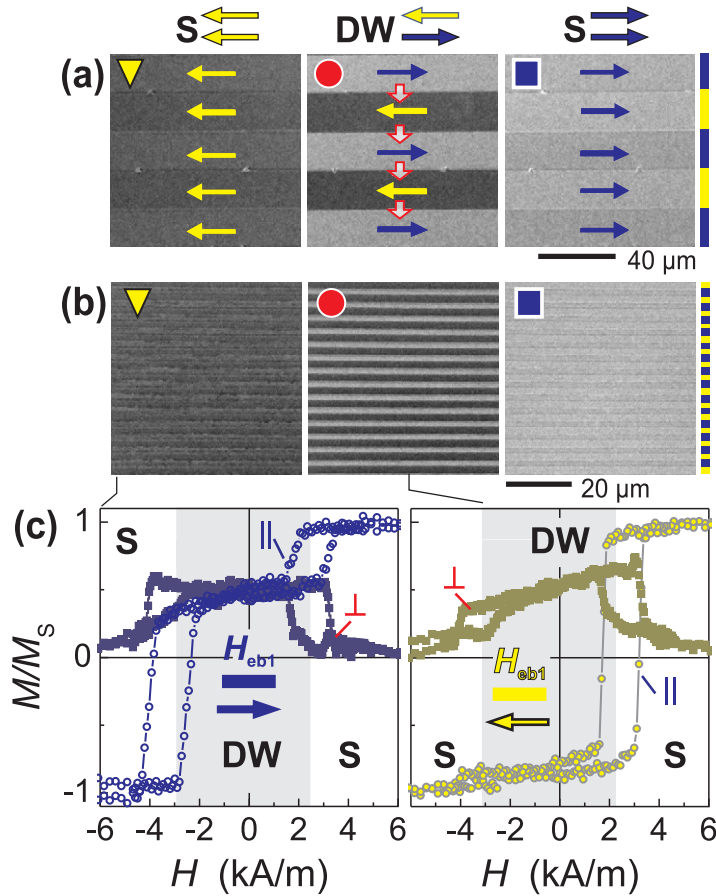
Figure 3. Representative domain states imaged by magneto-optical Kerr microscopy for the exchange bias modulation with the period (a) P_{st} of $40\,\mu m$ and (b) $4\,\mu m$, respectively. The S and DW states are indicated. (c) Longitudinal ($\parallel$) and transverse ($\perp$) sensitivity magneto-optical magnetization curves of the individual stripes with opposite orientation of exchange bias. (The ratio M/M_s is derived from the magneto-optical amplitude of the individual stripes at $\pm$ magnetic saturation.)

(cf similar structures in [25, 28, 29]). The difference in the step heights of the magnetic signal from $P_{st} = 40$ to $4\,\mu m$ is attributed to the photolithographic processing errors resulting in a non-equidistant stripe width as confirmed by atomic force microscopy (AFM) measurements [28]. Yet, the stripe periodicity P_{st} is retained. For further considerations, the true stripe fractions $\nu_{eb,dep}$ and $\nu_{eb,irr} = 1 - \nu_{eb,dep}$ for the as-deposited and implanted area will therefore be used.

The magnetic domain states are imaged by high resolution magneto-optical Kerr microscopy in the longitudinal mode [19], the results of which are displayed in figures 3(a) and (b). Magnetic saturation (S) is achieved at sufficiently high positive and negative magnetic fields. The visible small contrast in the S-state images is due to different magneto-optical contrast of the as-deposited and irradiated stripes. In accordance with the magnetization loop measurements, striped domain structures are found in the DW region. Despite the difference in P_{st} the domain states display alike characteristics. Locally magneto-optically measured magnetization loops of individual neighboring non-irradiated and irradiated stripes, including as well the transverse magnetization component ($\perp$), are shown in figure 3(c) for $P_{st} = 4\,\mu m$. Noticeable, a two step

reversal is seen in both longitudinal (||) loops. With the switching of one individual stripe region, also a change in the magnetization in the other phase stripes occurs, indicating a DW mediated coupling between the stripes' magnetization. The origin of this coupling becomes obvious from the transverse sensitivity curves. In the DW state a magnetization component perpendicular to the exchange bias axis and the applied magnetic field regions occurs. This is a direct result of the Néel-type DW structure with its extended magnetic tail region [19], which transversal magnetization component is probed by the transversal loop measurement. A canted transverse magnetization component exists for the DW magnetization alignment and with saturation (S) the transversal component extinguishes.

In spite of the similarity in the quasi-static magnetic properties for different stripe widths, the magnetic structuring results in significant differences on the dynamic magnetic properties. The dynamic permeability spectra of the exchange biased samples are recorded by means of a pulsed inductive microwave magnetometry setup [30]. The films are oriented with the unidirectional anisotropy axis parallel to the external bias field direction H_{bias} and perpendicular to the pulse field. As with the quasi-static investigations, all data reported below are obtained for a range of static bias fields from -6.4 to $6.4\,\mathrm{kA\,m^{-1}}$ along this axis (cf magnetization loop in figure 2). An in-plane magnetic field pulse H_{pulse} of about $160\,\mathrm{A\,m^{-1}}$ with a rise time of $t_{20/80} = 80\,\mathrm{ps}$ is used for the dynamic excitation. The same values are used for the micromagnetic simulations to follow. The permeability spectra $|\mu(f)|$ are obtained by Fourier transform of the time-domain signal [17, 31].

For the as-deposited film as well as stripe periods of $40\,\mu\mathrm{m}$ and $4\,\mu\mathrm{m}$ the recorded permeability spectra $|\mu(f)|$ are plotted as function of the external bias field H_{bias} (figure 4). For the stripe pattern with $P_{st} = 40\,\mu\mathrm{m}$ (figure 4(b)) the spectra exhibit two dominant resonance modes for almost all field values ($H_{bias} \neq 0\,\mathrm{kA\,m^{-1}}$). No significant influence of the DW state can be detected. The superposition of the extended 'as-deposited' and 'irradiated' exchange bias reference film frequencies $f_{res,dep}$ and $f_{res,irr}$ prove that the resonance modes are represented by the independent homogeneous excitation of each stripe fraction, each mode separately following a field-shifted Kittel-like behavior [11, 32]:

$$f_{eb1,2}^2 = \left(\frac{\gamma}{2\pi\mu_0}\right)^2 M_S \left[H_{k,F} + H_{dem,eff} \pm \left(H_{bias} - H_{eb}\right)\right] \tag{1}$$

with the saturation magnetization M_S, the gyromagnetic factor γ and the vacuum permeability μ_0. The effective field H_{eff} is determined by the magnetic film's anisotropy field $H_{k,F}$, the effective demagnetization field $H_{dem,eff}$, H_{bias} and H_{eb} being aligned with or opposite to H_{bias}. No coupling effects between the stripes are included here. $H_{dem,eff}$ depends on the patterning parameters of the film. A homogeneous local alignment of magnetization within the stripes is assumed.

Due to the comparable effective fields H_{eff}, i.e. identical ferromagnetic anisotropy field ($H_{k,F} = 0.4\,\mathrm{kA\,m^{-1}}$) and similar exchange bias field ($H_{eb,dep} = 3.6\,\mathrm{kA\,m^{-1}}$ and $H_{eb,irr} = 3.2\,\mathrm{kA\,m^{-1}}$), the as-deposited and irradiated films and thus the hybrid property film exhibit a crossing of the individual precessional frequencies at about zero field. The frequency minima shifted along the bias field axis of the regional film precessional frequencies f_{dep}^{full} and f_{irr}^{full} define the dynamic exchange bias field shift of the separate, yet laterally combined exchange bias systems.

For the reduced stripe period of $4\,\mu\mathrm{m}$ (figure 4(c)) the obtained $|\mu|$-spectrum is rather different. In contrast to the samples with large periodicity, the smaller structures exhibit a
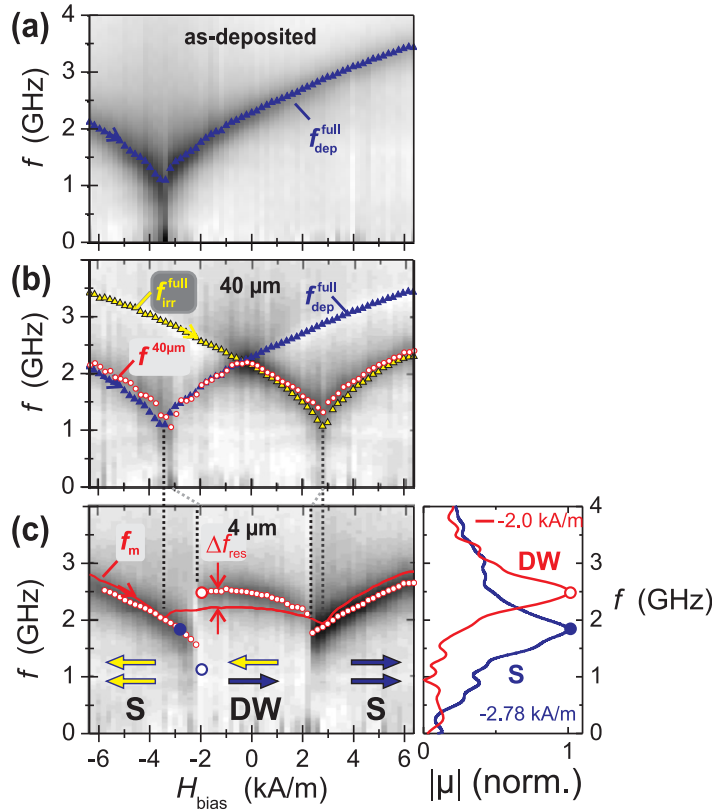
Figure 4. Dynamic permeability spectra $|\mu(H_{bias})|$ of the extended full film (a) in the as-deposited state and with alternating exchange bias modulation at a stripe period of (b) $40\,\mu$m and (c) $4\,\mu$m. For the broad stripes frequencies f_{dep}^{full} and f_{irr}^{full} of the extended reference films with as-deposited (dep) and ion modified exchange bias (irr) are overlayed as indicated. The hybrid frequency of the $4\,\mu$m structures in external saturation fields (S) is approximated by a collective frequency f_m resulting from the weighted full film precessional frequencies (equation (2), $\nu_{eb,dep} = 0.45$ from AFM analysis). The permeability spectra for $H_{bias} = -2.0\,\text{kA m}^{-1}$ (DW) and $H_{bias} = -2.78\,\text{kA m}^{-1}$ (S) are plotted in (c). (Calculated positions of resonance frequency for $H_{bias} = -2.0\,\text{kA m}^{-1}$ are indicated as open circles, cf figure 6.)

single collective resonance peak in the complete field region. For external bias fields ensuring a saturated (S) domain state ($|H_{bias}| > |H_{eb1,2}|$), the precessional frequencies' behavior again resembles a Kittel-type dependence. For the transition to the nominally antiparallel (DW) magnetization alignment a discontinuous frequency jump to smaller values occurs. Moreover, within this field range the field dependence of precessional frequency behavior is strongly reduced. The collective resonance frequency in the S phase region can be discussed within the framework of coupling induced by dynamic charges [33] at the magnetic phase boundary. Even though for saturated stripes only the homogeneous acoustic mode might be expected, the differing effective fields $H_{eff1/2}$ due to the locally opposite exchange bias directions for each separate stripe fraction lead to slightly different individual precessional frequencies. Thus, magnetization components perpendicular to the stripe interfaces ($m_y(t)$) and dynamic demagnetization effects ($H_{dem,eff} = (m_{y1}(t) - m_{y2}(t))N_{eff}M_s$) contribute, similar as for the case

of DW induced dynamic charges [33]. As a consequence the time dependent charges couple for reduced dimensions and increased amount of interfaces. The synchronized frequency f_m (cf figure 4(c), S) can be approximated by weighting the initial precessional frequencies of the extended films taking the real stripe fractions ν_i into account to

$$f_\text{m} = \nu_\text{eb,dep} \times f_\text{dep}^\text{full} + (1 - \nu_\text{eb,dep}) \times f_\text{irr}^\text{full}. \tag{2}$$

A deviation of the assumed f_m dependence for external bias fields around the frequency minima occurs as the DW region narrows for smaller stripe widths (compare figures 6(b) and (c)). The switching of the individual stripes occurs at field values $H_\text{bias} < \pm H_\text{eb1,2}$. The narrowing of the DW region, respectively, the decrease of the effective exchange bias field amplitudes, is attributed to the additional DW energy contribution [29], increasing with higher DW density and for smaller stripe width. Yet, opposite to the S mode the frequencies are shifted up in comparison to the merged precessional frequency f_m (see figure 4(c), Δf_res), which indicates a change $H_\text{dem,eff}$ in the structured film for the DW state. The interplay of the local effective changes in H_eff with the modification in the magnetically charged magnetic configurations, the associated local tilting of magnetization, the effects of different exchange coupling across the stripes, and the magneto-static interactions are not accessible easily by analytical models.

Therefore, in order to elucidate the different behavior of the S and the DW phase, the dynamics of the two configurations are calculated by means of micromagnetic simulations [34]. The cell size for the calculations is chosen to be 5 nm. In accordance to the experimental data, the ferromagnetic anisotropy field of $\text{Ni}_{81}\text{Fe}_{19}$ ($J_\text{s} = 1\,\text{T}$) was set $H_\text{k,F} = 0.4\,\text{kA m}^{-1}$ and the regions of local exchange bias fields (H_eb1 and H_eb2) are set in accordance to the real stripe widths. Full film simulation is realized by the implementation of periodic boundary conditions in the film plane (x, y).

The relaxed magnetization configurations for an external bias field of $H_\text{bias} = 0$ for $P_\text{st} = 20$ and $4\,\mu\text{m}$ are displayed in figure 5. In agreement with the experimental data (figure 3) the plots of the normalized in-plane magnetization components m_x and m_y illustrate a considerable canting of the effective magnetization within the stripe center due to the Néel walls positioned at the stripe interfaces for $P_\text{st} = 4\,\mu\text{m}$. This is also in agreement with magneto-optical investigations on similar samples [25]. A transverse magnetization component exists for the antiparallel magnetization alignment because of the extended and overlapping Néel wall tails of the imprinted DWs.

The simulated magnetization dynamics of the S and DW states at an applied external bias field of $H_\text{bias} = -2.0\,\text{kA m}^{-1}$ are compared to the experimentally accessible permeability spectra (figure 6). For a stripe period of $20\,\mu\text{m}$ two peaks in the DW state become visible, differing in accordance to the additional local exchange bias field being aligned parallel or opposite to the magnetic bias field. For the small stripe width, the calculated spectra support the existence of a merged single mode resonance behavior for the S and DW state. For the DW configuration the simulated resonance peak position at a precessional frequency of $f_\text{DW,sim}(-2.0\,\text{kA m}^{-1}) = 2.5\,\text{GHz}$ resembles the experimental value of $f_\text{DW,exp}(-2.0\,\text{kA m}^{-1}) = 2.5\,\text{GHz}$. The simulation of the S state at an identical bias field with $f_\text{DW,exp}(-2.0\,\text{kA m}^{-1}) = 1.1\,\text{GHz}$ affirms the experimentally found drastic frequency drop upon elimination of the DWs in the S state. The difference in precessional frequency $\Delta f_\text{S,sim}$ is $1.4\,\text{GHz}$. Yet, a deviation from the experimental data remains. One cause for the deviation of experiment and simulation is a direct consequence of neglecting possible rotational anisotropy contributions in
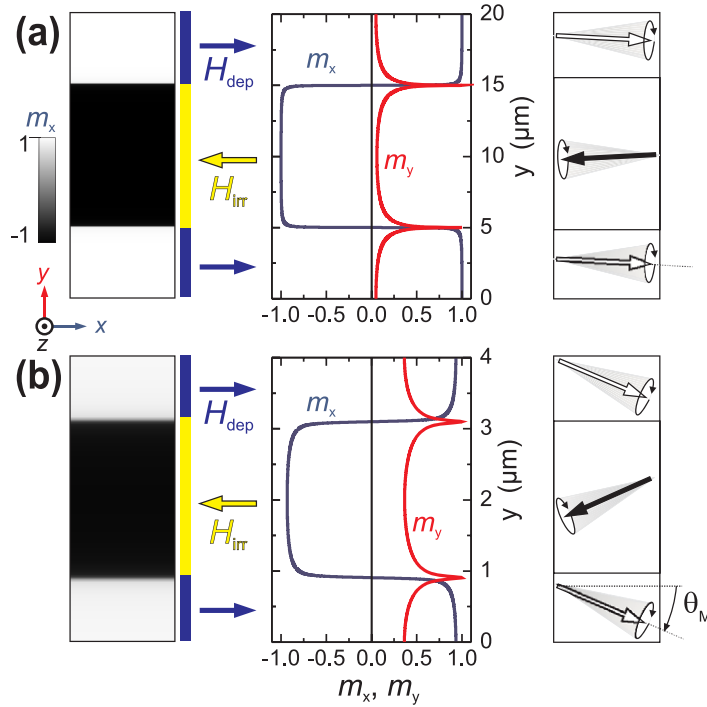
Figure 5. Simulated domain state for the DW state of (a) a 20 μm and (b) a 4 μm stripe period in zero external bias field. The according magnetization components along the stripe (m_x) and perpendicular to the interface (m_y) are plotted. The resulting magnetization configurations for the dynamic excitation are sketched.
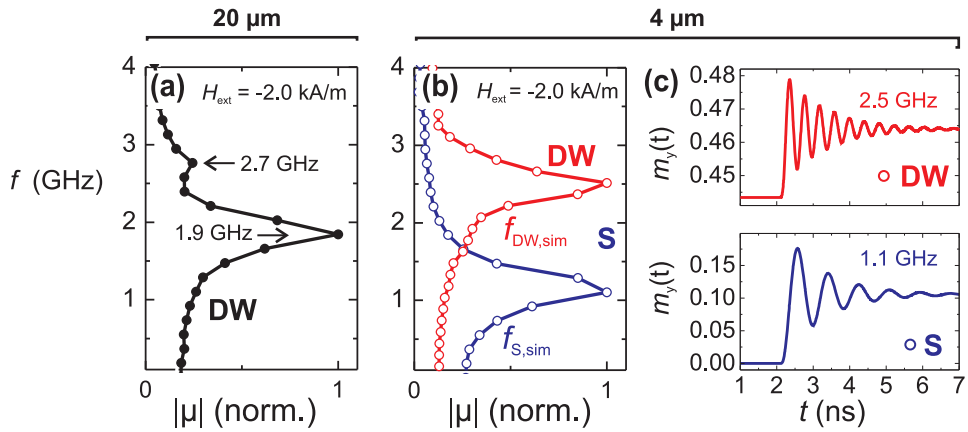
Figure 6. Simulated normalized permeability spectra for the S and DW state for a P_{st} of (a) 20 μm and (b) of 4 μm. The same magnetic bias field value $H_{bias} = -2.0\,\text{kA}\,\text{m}^{-1}$ is used for all the simulations. The magnetization pulse response for the S and DW state of the narrow stripe width is shown in (c). f_{res} for the DW and S states are given in (a) and (c).

the simulations [25] that for exchange biased systems add an additional dynamic anisotropy term and thus increase in f_{res}, which is not easy to model by micromagnetic simulations. An additional reason for the found discrepancy lies in the interfacial stripe structure that is
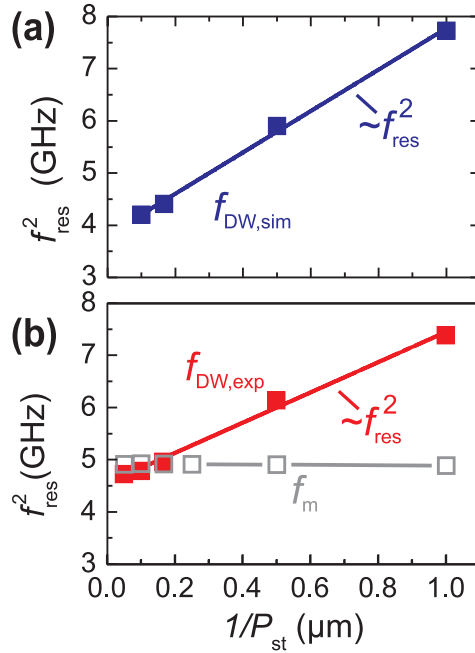
Figure 7. Change of precessional frequency square f_{res}^2 with stripe width from (a) simulation ($f_{DW,sim}$) and (b) experiment ($f_{DW,exp}$) in zero external field and for antiparallel stripe magnetization. The common mode value f_m is added in (b).

assumed to be exactly abrupt for the micromagnetic simulations, but will have a certain (but unknown) width for the processed samples. Another reason lies in differences in the calculated and actual exhibited micromagnetic structure. Comparing the overall tilting of magnetization of the experimentally obtained overall transverse magnetization component ($\overline{m}_y \approx 0.5$) and of the simulated DW structure ($\overline{m}_y \approx 0.43$) reveals a stronger tilting of magnetization in the real structures. Nevertheless, the simulated permeability of the S state confirms the decrease of f_{res} as compared to the DW state. Consequently, for identical external bias fields and thus nominally identical effective fields acting onto the separate stripe volumes, the simulation clearly reveals that the frequency increase results from the inhomogeneous DW magnetization configuration with canted distribution of magnetization. The direct ferromagnetic coupling, i.e. Néel walls at the stripe interface, acts as an additional intrinsic transverse field contribution H_{trans} [35].

A comparison of the experimentally obtained and simulated resonance frequencies $f_{DW,exp}$ and $f_{DW,sim}$ at zero external field as a function of the reciprocal stripe period is given in figure 7, now also including other stripe widths. In the experiment, with decreasing period and thus increasing Néel wall density the resonance frequency increases in comparison to the weighted merged frequency in zero external field f_m (cf figure 4(c)). The simulated change in f_{res} for the DW magnetization configurations qualitatively agrees with the experimental data. For smaller periods the dynamics are dominated by DW effects and f_{res} increases strongly. The shown linear dependence of f_{res}^2 versus the reciprocal stripe period P_{st} in figure 7 points to an effective shape anisotropy contribution with an effective demagnetization factor N_{eff} changing with $1/P_{st}$. Yet, a small discrepancy between the experimental and simulated slope f_{res}^2/P_{st} exists, but the general dependence is confirmed.

3. Conclusions

The results show that the precessional frequency of magnetic thin films can be influenced by means of direct high density DW imprinting. The dynamic magnetic response in exchange biased $Ni_{81}Fe_{19}$/IrMn magnetic thin films is tuned by imprinting periodic DW patterns with overlapping DW structures through selective ion irradiation. Mode coupling via dynamic magnetic charges in the periodically modulated magnetization patterns is directly provoked by adjusting the micromagnetic interface density. For high DW densities an increased precessional frequency is achieved. For large periods the dynamic behavior resembles a mere superposition of the initial frequencies of the extended reference films, i.e. the structures exhibit a bimodal permeability spectrum. Yet, for reduced periods the spectra become monomodal with a common precessional frequency. At the nearly abrupt transition from the saturated magnetic phase to the DW phase the permeability spectra exhibit a pronounced discontinuous jump in the dynamic response, making an abrupt switch between two different dynamic states achievable. The controlled introduction of high density and overlapping micromagnetic objects is a novel way to tailor the dynamic magnetic properties of magnetic thin films.

Acknowledgments

References

[1] Thompson D A and Best J S 2000 *IBM J. Res. Dev.* **44** 311–22
[2] Gardner D S, Schrom G, Hazucha P, Paillet F, Karnik T and Borkar S 2007 *IEEE Trans. Magn.* **43** 2615–7
[3] Wu H, Gardner D S, Xu W and Yu H B 2012 *IEEE Trans. Magn.* **48** 4123–6
[4] Ikeda S, Nagae T, Shimada Y, Kim K H and Yamaguchi M 2006 *J. Appl. Phys.* **99** 08P507
[5] Muroga S, Asazuma Y, Endo Y, Shimada Y and Yamaguchi M 2012 *IEEE Trans. Magn.* **48** 4320–3
[6] Kruglyak V V, Demokritov S O and Grundler D 2010 *J. Phys. D: Appl. Phys.* **43** 264001
[7] Adeyeye A O and Jain S 2011 *J. Appl. Phys.* **109** 07B903
[8] Lenk B, Ulrichs H, Garbs F and Münzenberg M 2011 *Phys. Rep.* **507** 107–36
[9] Chumak A V, Karenowska A D, Serga A A and Hillebrands B 2013 *Magnonics: From Fundamentals to Applications* vol 125 ed S O Demokritov and A N Slavin (Berlin: Springer) pp 243–57
[10] McMichael R, Stiles M, Chen P and Egelhoff W F 1998 *Phys. Rev.* B **58** 8605–12
[11] McCord J, Mattheis R and Elefant D 2004 *Phys. Rev.* B **70** 094420
[12] McCord J, Kaltofen R, Schmidt O G and Schultz L 2008 *Appl. Phys. Lett.* **92** 162506
[13] Topp J, Heitmann D, Kostylev M P and Grundler D 2010 *Phys. Rev. Lett.* **104** 207205
[14] Ding J, Kostylev M and Adeyeye A O 2011 *Phys. Rev. Lett.* **107** 047205
[15] Walowski J, Kaufmann M D, Lenk B, Hamann C, McCord J and Münzenberg M 2008 *J. Phys. D: Appl. Phys.* **41** 164016
[16] Patschureck C, Lenz K, Liedke M O, Lutz M U, Strache T, Mönch I, Schäfer R, Schultz L and McCord J 2012 *Phys. Rev.* B **86** 054426
[17] Queitsch U, McCord J, Neudert A, Schäfer R, Schultz L, Rott K and Brückl H 2006 *J. Appl. Phys.* **100** 093911
[18] Duerr G, Huber R and Grundler D 2012 *J. Phys.: Condens. Matter* **24** 024218

[19] Hubert A and Schäfer R 1998 *Magnetic Domains—The Analysis of Magnetic Microstructures* (Berlin: Springer)

[20] Meiklejohn W H and Bean C P 1956 *Phys. Rev.* **102** 1413–4

[21] Berkowitz A E and Takano K 1999 *J. Magn. Magn. Mater.* **200** 552–70

[22] Fassbender J, Ravelosona D and Samson Y 2004 *J. Phys. D: Appl. Phys.* **37** R179–R196

[23] Fassbender J and McCord J 2008 *J. Magn. Magn. Mater.* **320** 579–96

[24] Ehresmann A, Krug I, Kronenberger A, Ehlers A and Engel D 2004 *J. Magn. Magn. Mater.* **280** 369–76

[25] McCord J, Schäfer R, Theis-Bröhl K, Zabel H, Schmalhorst J, Höink V, Brückl H, Weis T, Engel D and Ehresmann A 2005 *J. Appl. Phys.* **97** 10K102

[26] Ziegler J, Ziegler M and Biersack J 2008 SRIM 200804 Code *The Stopping and Range of Ions in Solids* (www.srim.org)

[27] Mougin A, Mewes T, Jung M, Engel D, Ehresmann A, Schmoranzer H, Fassbender J and Hillebrands B 2001 *Phys. Rev.* B **63** 060409

[28] Hamann C, Mönch I, Kaltofen R, Schäfer R, Gemming T, Schultz L and McCord J 2008 *J. Appl. Phys.* **104** 013926

[29] McCord J, Schultz L and Fassbender J 2008 *Adv. Mater.* **20** 2090–3

[30] T J, Silva C S, Lee T M C and Rogers C T 1999 *J. Appl. Phys.* **85** 7849–62

[31] Kos A B, Silva T J and Kabos P 2002 *Rev. Sci. Instrum.* **73** 3563–9

[32] Kittel C 1948 *Phys. Rev.* **73** 155

[33] Polder D and Smit J 1953 *Rev. Mod. Phys* **25** 89

[34] Berkov D Version D61 extended 2010 *MicroMagus* (www.micromagus.de)

[35] Hamann C, McCord J, Schultz L, Toperverg B P, Theis-Bröhl K, Wolff M, Kaltofen R and Mönch I 2010 *Phys. Rev.* B **81** 024420